Hydrogen evolution at catalytically-modified nickel foam in alkaline solution

Boguslaw Pierozynski [a, *], Tomasz Mikolajczyk [a], Ireneusz M. Kowalski [b]

[a] Department of Chemistry, Faculty of Environmental Management and Agriculture, University of Warmia and Mazury in Olsztyn, Plac Lodzki 4, 10-957 Olsztyn, Poland
[b] Department of Rehabilitation, Faculty of Medical Sciences, University of Warmia and Mazury in Olsztyn, Zolnierska 14C Street, 10-561 Olsztyn, Poland

HIGHLIGHTS

- Nanoparticles of Pd or Ru enhanced kinetics of HER on Ni foam.
- Pd and Ru modified electrochemically active surface of Ni foam.
- Pd/Ru-modified Ni foam to make cathodes for alkaline water electrolysers.

ARTICLE INFO

ABSTRACT

This work reports on hydrogen evolution reaction (HER) studied at catalytically modified nickel foam material. The HER was examined in 0.1 M NaOH solution on as received, as well as for Pd and Ru-activated nickel foam catalyst materials, produced via spontaneous deposition of trace amounts of these elements. Catalytic modification of nickel foam results in significant facilitation of the HER kinetics, as manifested through considerably reduced, a.c. impedance-derived values of charge-transfer resistance parameter and substantially altered Tafel polarization slopes. The presence of catalytic additives is clearly revealed through hydrogen underpotential deposition (H UPD) phenomenon, as well as spectroscopically from SEM (Scanning Electron Microscopy) analysis.

© 2014 Elsevier B.V. All rights reserved.

1. Introduction

The process of hydrogen evolution at metal electrodes is one of the most important electrochemical reactions, especially with respect to fast development of PEM (Proton Exchange Membrane) fuel-cell and battery technologies. Nickel is well-known for being one of the best, non-noble catalyst materials for hydrogen evolution reaction (HER) in alkaline media. This is primarily because Ni is exclusively resistant to corrosion at high pH values [1–5]. Of special importance are nickel structures having large specific surface area (large roughness); these include: Ni-sintered nanoparticle materials [6–8], nickel-coated carbon fibre/felt [9–12] and electrocatalysts based on nickel foam [13,14]. Nickel foams are typically produced by chemical vapour deposition (CVD) [15],

electrochemical or electroless deposition method with a polyurethane foam precursor [16]. Such-produced Ni foam makes highly-valuable electrocatalyst material having not only high porosity and specific surface area, but also good electrical conductivity, high corrosion resistance and superior mechanical properties [14,16].

In addition, significant improvement of electrocatalytic properties of nickel foam (e.g. towards HER or oxidation of aliphatic alcohols) could conveniently be realized through surface deposition of nano-structured noble metals (for example: Pd, Ru, Rh or Pt), either in a single element arrangement or as binary/ternary alloys (see Ref. [14] and other papers quoted there). The above might be carried-out by means of electrodeposition, spontaneous deposition [14,17,18] or by chemical reduction processes, where the latter are typically facilitated with $NaBH_4$, ethylene glycol, hydrazine or their compositions [19–23].

In this work, Pd and Ru-modified nickel foam catalyst materials were prepared via spontaneous deposition methods (see

* Corresponding author. Tel.: +48 89 523 4177; fax: +48 89 523 4801.
E-mail addresses: bogpierozynski@yahoo.ca, boguslaw.pierozynski@uwm.edu.pl (B. Pierozynski).

Refs. [14,17,18]), in order to produce cathodes having superior HER performance in alkaline environments.

2. Experimental

2.1. Solutions, chemical reagents, electrodes and electrochemical cell

All solutions were prepared using a Direct-Q3 UV ultra-pure water purification system from Millipore (18.2 MΩ cm water resistivity). 0.1 M NaOH supporting solution was prepared from AESAR, 99.996% NaOH pellets. In addition, 0.5 M H_2SO_4 solution was made up from sulphuric acid of highest purity available (SEASTAR Chemicals, BC, Canada) for periodical charging of a Pd reversible hydrogen electrode.

An electrochemical cell, made of Pyrex glass, was used during the course of this work. The cell comprised three electrodes: a Ni foam-based working electrode (WE) in a central part, a reversible Pd hydrogen electrode (RHE) as reference and a Pt counter electrode (CE), both placed in separate compartments. Before conducting the HER experiments each Ni foam electrode was additionally activated in 0.1 M NaOH by cathodic polarization at 20 mA for 300 s in order to remove any spontaneously formed Ni oxide layer.

Nickel foam was delivered by MTI Corporation (purity: > 99.99% Ni; thickness: 1.6 mm; surface density: 346 g m^{-2}; porosity: ≥ 95%), whereas all examined electrodes were 1 cm × 1 cm. Spontaneous depositions of Pd and Ru catalysts on nickel foam samples were carried-out according to the corresponding descriptions given in Ref. [14] (for palladium) and Refs. [17,18] for ruthenium. In brief, freshly cut foam samples were subjected to acetone and CH_2Cl_2 wash (both for 15 min + ultrasonication), following air drying and acid etching in 2 M HCl (for 15 min at 60 °C). Then, spontaneous deposition of metal catalysts was realized by dipping such pretreated foam electrodes in 0.005 M $PdCl_2$ (pH = 1.0, $t_{dep.}$ = 15–300 s, temp. = 25 ± 1 °C) and 0.001 M $RuCl_3$ (pH = 1.0, $t_{dep.}$ = 15–60 min, temp. = 20–30 °C) to obtain Pd and Ru-modified Ni foam catalysts, respectively. The palladium RHE was made of a coiled Pd wire (0.5 mm diameter, 99.9% purity, Aldrich) and sealed in soft glass. Before its use, this electrode was cleaned in hot, concentrated sulphuric acid, followed by cathodic charging with hydrogen in 0.5 M H_2SO_4, until H_2 bubbles in the electrolyte were clearly visible. The stability of the Pd reference electrode was occasionally checked by recording its potential shift in time. Thus, all the potentials throughout this work are given on the RHE scale. A counter electrode was made of a coiled Pt wire (1.0 mm diameter, 99.9998% purity, Johnson Matthey, Inc.). Prior to its use, the counter electrode was cleaned in hot sulphuric acid or was flame-annealed. Similarly, before each series of experiments, the electrochemical cell was taken apart and soaked in hot sulphuric acid for at least 3 h. After having been cooled to about 30 °C, the cell was thoroughly rinsed with Millipore ultra-pure water. Atmospheric oxygen was removed from solution before each experiment by bubbling with high-purity argon (Ar 6.0 grade from Linde). In addition, during the experiments, the argon gas flow was kept above the solution.

2.2. Experimental methodology

Electrochemical impedance spectroscopy, cyclic voltammetry and quasi steady-state polarization techniques were employed during the course of this work. All measurements were performed at room temperature: 22 °C by means of the *Solartron* 12,608 W Full Electrochemical System, consisting of 1260 frequency response analyzer (FRA) and 1287 electrochemical interface (EI).

For a.c. impedance measurements, the generator provided an output signal of 5 mV and the frequency range was swept between 1.0×10^5 and 0.5×10^{-1} Hz. The instruments were controlled by *ZPlot 2.9* or *Corrware 2.9* software for Windows (Scribner Associates, Inc.). Usually, three impedance measurements were conducted at each potential value, independently at two foam electrodes. Reproducibility of such-obtained results was typically below 10%. Data analysis was performed with *ZView 2.9* (*Corrview 2.9*) software package, where the impedance spectra were fitted by means of a complex, non-linear, least-squares immitance fitting program, *LEVM 6*, written by J.R. Macdonald [24]. Also, a quasi-potentiostatic cathodic polarization experiments (recorded at a scan rate of 0.5 mV s^{-1}) for the HER were carried-out at all Ni foam electrodes.

In addition, spectroscopic characterization of baseline Ni foam, Pd, and Ru-activated Ni foam electrodes was performed by means of Quanta FEG 250 scanning electron microscope (SEM). Furthermore, powder XRD (X-ray diffraction) technique was employed to determine average sizes of Pd and Ru crystallite domains for the selected Pd and Ru-modified Ni foam samples. The XRD spectra were recorded by means of Siemens D500 powder diffractometer with CuK$_\alpha$ radiation (λ = 1.5418 Å, U = 38 kV, I = 30 mA). Also, EDX identification of ruthenium element for Ru-modified nickel foam electrodes was carried-out by means of Hitachi S3400 SEM/EDX equipment, at an acceleration voltage of 20 kV.

3. Results and discussion

3.1. SEM and XRD characterizations of Pd and Ru-modified nickel foam electrodes

Fig. 1a and b below present SEM micrograph pictures of MTI-manufactured nickel foam, at 100 × and 1000 × magnifications, correspondingly. On the other hand, Fig. 1c and d illustrate the effect of spontaneous deposition of palladium at very low level (*ca.* 0.1 wt.% Pd) on the MTI foam, recorded for the magnifications of 100 × and 15,000 ×, respectively. Hence, at the magnification of 15,000 ×, a high-density of homogeneously distributed small Pd nuclei can clearly be seen in Fig. 1d. Similarly, Fig. 1e and f illustrate SEM micrograph pictures recorded for Ru-modified (*ca.* 0.1 wt.% Ru) MTI nickel foam, at the magnifications of 100 × and 15,000 ×, respectively. Here, in contrast to palladium, ruthenium deposit forms a discontinuous catalyst layer islands over the nickel foam surface (see Fig. 1f). In addition, quantities of the deposited catalysts on the nickel foam substrate were assessed by means of a weighing method.

Fig. 2a and b below present a comparison of the X-ray diffraction patterns for spontaneously deposited Pd and Ru elements on the Ni foam substrate, correspondingly.

Thus, the powder XRD-calculated average Pd grain size value came to 7 nm, while Ru crystallites could not be identified (see Fig. 2b again), most likely due to insufficient amount of ruthenium present in the structure. However, Ru detection was successfully achieved by the EDX analysis (see Fig. 2c), which confirmed the presence of ruthenium on the order of 0.22 ± 0.03 wt.% within the composite.

3.2. A.C. impedance characteristics of HER on pure and catalyst-modified Ni foam materials in 0.1 M NaOH

A.c. impedance characterization of the HER on pure Ni foam and catalyst (Pd, Ru)-modified Ni foam electrodes in 0.1 M NaOH is shown in Fig. 3a and b, and Table 1. Thus, the impedance-examined, unmodified Ni foam electrode exhibited single, "depressed" semicircles (a single-step charge-transfer reaction) at all potentials, in
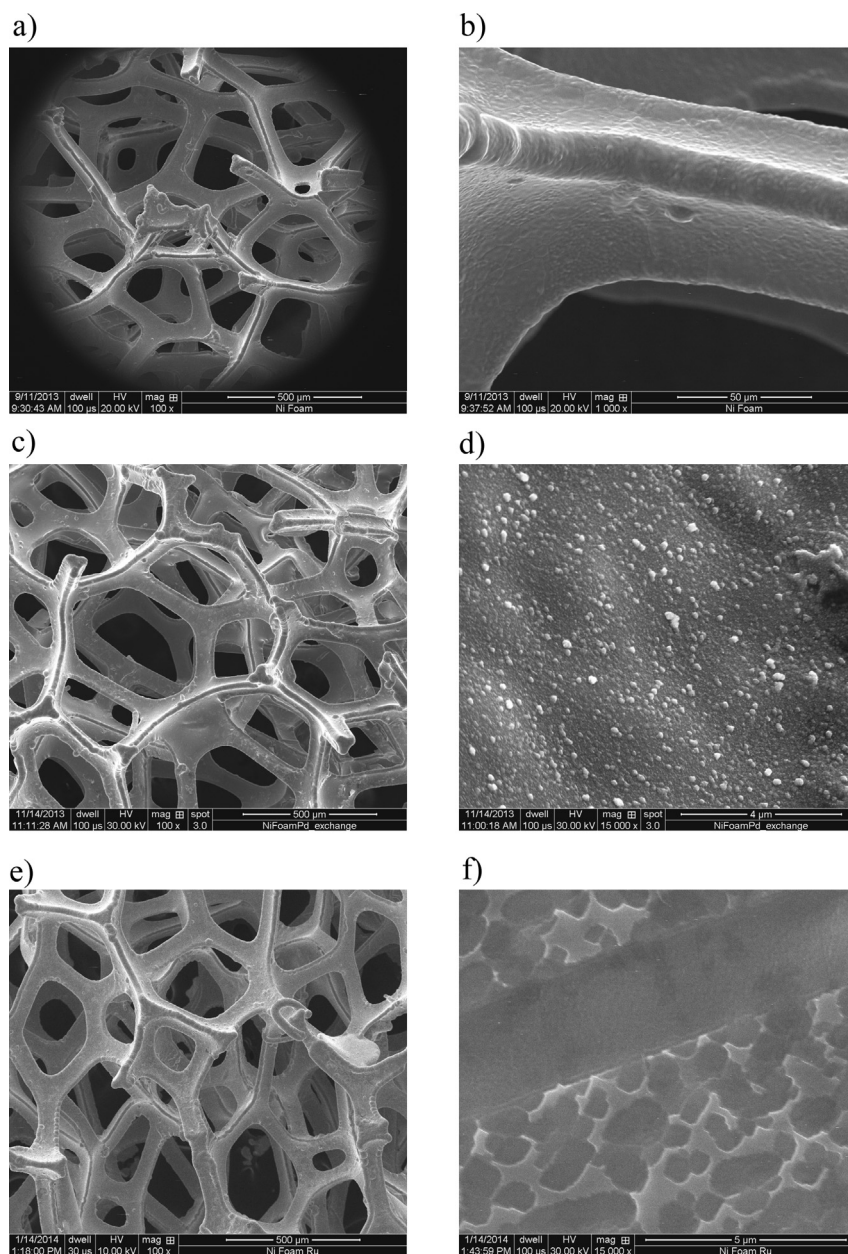
a)

b)

c)

d)

e)

f)

Fig. 1. a) SEM micrograph picture of pure Ni foam surface, taken at 100 magnification; b) as in (a), but taken at 1000 magnification; c) as in (a), but for Pd-modified Ni foam surface (*ca.* 0.1 wt.% Pd); d) As in (c), but taken at 15,000 magnification; e) as in (a), but for Ru-modified Ni foam surface (*ca.* 0.1 wt.% Ru); f) as in (e), but taken at 15,000 magnification.

the explored frequency range (see examples of Nyquist impedance plots in Fig. 3a). The overpotential dependence of Faradaic reaction resistance (R_{ct}) and double-layer capacitance (C_{dl}) parameters for the HER at pure nickel foam (derived based on a constant phase element − CPE-modified Randles equivalent circuit model shown in Fig. 4a) is presented in Table 1. The CPE element was used in the circuit in order to account for the capacitance dispersion [25,26] effect, represented by distorted semicircles in the Nyquist imped-ance plots.

Hence, for the cathodically activated Ni foam electrodes the recorded R_{ct} parameter decreased from 14.40 Ω g at −50 mV to 0.18 Ω g at the potential of −400 mV vs. RHE. Simultaneously, the C_{dl} parameter diminished from 8341 to 3166 μF g^{-1} for the same potential span. The latter effect most likely results from partial blocking of electrochemically active electrode surface by freshly formed H$_2$ bubbles, something that could easily be visualized for a

complex Ni foam electrode structure (see Fig. 1a), especially at increased cathodic overpotentials. Please note that when the capacitance value of 8341 μF g^{-1} (recorded for electrode weight of 33.4 mg at −50 mV RHE) is referred to that commonly used value of 20 μF cm^{-2} in literature for smooth and homogeneous surfaces [27,28], electrochemically active surface area of the Ni foam elec-trode could roughly be estimated at 13.9 cm^2.

On the other hand, the HER electrochemical impedance behaviour of both the Pd and the Ru-activated Ni foam electrodes is characterized by two "depressed", partial semicircles, clearly discernible in the impedance plots at all examined electrode po-tentials (see examples of the recorded Nyquist impedance plots in Fig. 3b). Here, a circuit model containing two CPE−R elements (Fig. 4b) was employed to characterize the recorded impedance behaviour, where the high-frequency semicircle (CPE$_p$−R$_p$) is usu-ally overpotential independent and it corresponds to the porosity of
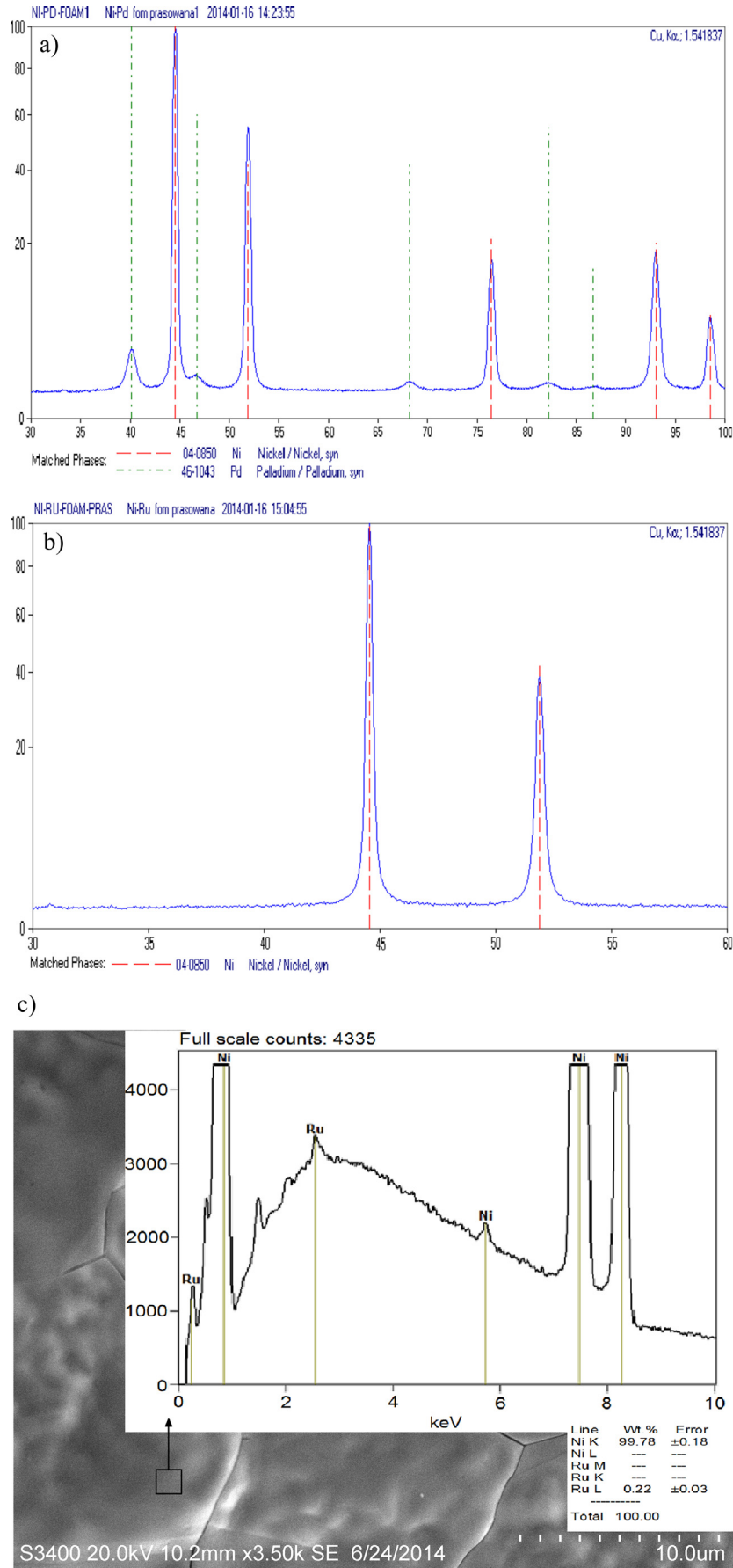
Fig. 2. Comparison of XRD patterns for spontaneously deposited Pd (a) and Ru (b) elements on nickel foam substrate, where observed diffraction lines correspond to the following sequence of fcc indices: (111), (200), (220), (311) and (222) for both Ni and Pd elements; c) SEM micrograph picture and its corresponding EDX spectrum for Ru-modified Ni foam substrate.
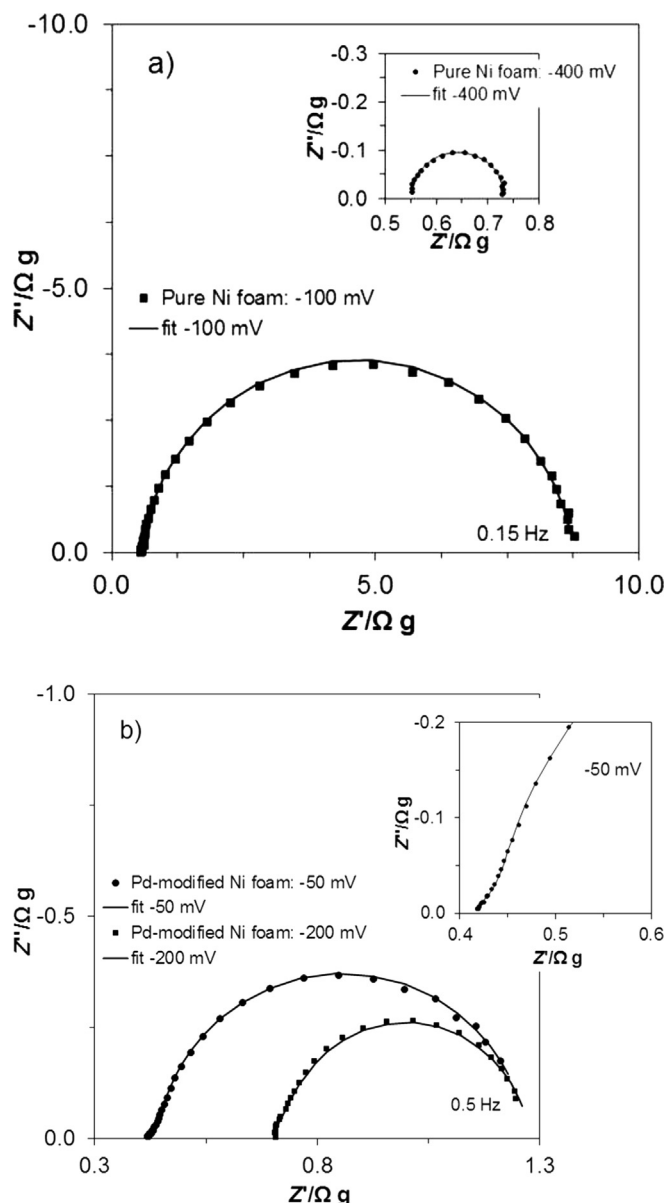
Fig. 3. a) Complex-plane impedance plots for the HER on pure Ni foam electrode surface in contact with 0.1 M NaOH, recorded at room temperature for the stated potential values (vs. RHE). The solid lines correspond to representation of the data according to the equivalent circuit shown in Fig. 4a; b) as above, but recorded on Pd-modified Ni foam electrode surface for potential values of −50 and −200 mV vs. RHE in reference to the equivalent circuit shown in Fig. 4b.

the electrode, whereas the low-frequency semicircle (CPE$_{dl}$–R_{ct}) is related to the kinetics of the hydrogen evolution reaction [6,8,12,29].

Hence, the recorded charge transfer resistance parameter for the Pd and the Ru-modified Ni foam electrodes ranged from 0.83 to 0.09 Ω g and 0.36 to 0.09 Ω g for the overpotential range: 50–400 mV RHE, respectively. The above means significant reduction of the R_{ct} parameter (as compared to those R_{ct} values recorded for the unmodified Ni foam surface), namely by 17 × and 40 × at −50 mV, and by 2 × at −400 mV for the Pd and the Ru-modified catalyst materials, respectively (see Table 1 for details). On the other hand, a radius of the high-frequency semicircle (implied surface porosity impedance response) was fairly potential-independent, which resulted in a relatively constant value of R_p parameter: 0.03–0.04 Ω g for the palladium-based and

0.03–0.13 Ω g for the Ru-modified Ni foam electrodes for the overpotential range: 50–400 mV (also, refer to the respective values of pseudocapacitance parameter, C_p in Table 1).

Furthermore, deposition of catalytic nanostructures (see Fig. 1d) resulted in a considerable enhancement of electrochemically accessible surface area. The above could conveniently be supported through the cyclic voltammetry behaviour presented comparatively for the baseline and the Ru-modified Ni foam materials in Fig. 5. Hence, substantial surface modification for the ruthenium-modified Ni foam is revealed through significantly increased current-density within the corresponding CV profile. In addition, unlike for the pure Ni foam, the Ru-modified CV profile commences with an extensive HOR anodic peak (*ca.* 0.20–0.50 V), while over a cathodic sweep an onset of the HER is clearly observed just positive to the reversible potential (significant HER facilitation, as compared to the unmodified Ni foam).

The recorded values of the C_{dl} parameter at −50 mV RHE came to 183,662 μF g^{-1} (Pd-modified Ni foam) and 95,558 μF g^{-1} for the Ru-based Ni foam catalyst material (*ca.* 22 × and 11 × increased active surface area of the composite electrodes, as compared to the baseline Ni foam cathode, respectively). When these surface ratios are referred to the calculated above ratios of the R_{ct} parameter, it becomes clear that superior HER performance was exhibited by the ruthenium-activated nickel foam cathode. However, at room temperature there might still be limited access to the large catalytic surface within the porous structure of the Pd-modified Ni foam electrode, including significant problems with unrestricted hydrogen bubble removal. One should note that similar phenomenon describing the influence of catalyst morphology and the role of gas bubble formation on the electrocatalysis of the cathodic hydrogen evolution reaction was comprehensively discussed in relevant literature, see for example Refs. [30–34].

Understandably, for the catalyst-modified nickel foam materials, the C_{dl} parameter exhibited similar (decreasing) overpotential dependence to that recorded for the baseline Ni foam electrode. In addition, dimensionless φ_1, φ_2 and φ_3 parameters (φ determines the constant phase angle in the complex-plane plot and $0 \le \varphi \le 1$) of the CPE circuits (see Fig. 4a and b) varied between: 0.90–0.98, 0.93–0.99 and 0.54–0.80, correspondingly.

Based on the linear relationship: −log R_{ct} vs. overpotential (for kinetically controlled reactions), exhibited here over the studied overpotential range: 50–400 mV vs. RHE, the exchange current-densities for the HER were calculated based on the Butler–Volmer equation and through utilization of the relation between the exchange current-density (j_0) and the R_{ct} parameter for overpotential approaching zero value [5,35–37]. Hence, the calculated values of the j_0 came to: 1.4 × 10^{-6}, 2.2 × 10^{-5} and 8.2 × 10^{-5} A cm^{-2} for the unmodified Ni foam, the Pd-based and the Ru-modified nickel foam catalyst materials, correspondingly.

3.3. H UPD phenomenon at Ru-modified Ni foam material

The presence of catalytic additives (Pd and Ru elements) on the surface of Ni foam electrodes was also revealed through the phenomenon of hydrogen underpotential deposition (H UPD) on metal substrates [38–42]. However, as the process of UPD of H on Pd is simultaneously accompanied by direct H absorption and by hydrogen overpotential deposition (H OPD) phenomena [43,44], the discussion of the process of UPD of H is limited here to the Ru-modified Ni foam catalyst.

Hence, the impedance characterization of the H UPD process at the Ru-modified Ni foam electrode, carried-out over the potential range: 50–150 mV vs. RHE (in order to avoid surface oxidation of Ru, see Refs. [45,46]), resulted in a partial and somewhat

Table 1
Electrochemical parameters for the HER, obtained on cathodically activated pure Ni foam, Pd and Ru-modified Ni foam electrodes in contact with 0.1 M NaOH. The results were obtained by fitting the CPE-modified Randles (Fig. 4a) and the two CPE–R element (Fig. 4b) equivalent circuits to the experimentally obtained impedance data (reproducibility usually below 10%, $\chi^2 = 5 \times 10^{-5}$ to 2×10^{-3}).

E/mV	R_{ct}/Ω g	C_{dl}/μF g^{-1}		
Pure Ni foam				
−50	14.40 ± 0.08	8341 ± 90		
−100	8.17 ± 0.02	7069 ± 52		
−150	2.91 ± 0.01	5596 ± 89		
−200	1.12 ± 0.01	4855 ± 156		
−250	0.56 ± 0.00	4192 ± 215		
−300	0.40 ± 0.00	4027 ± 302		
−350	0.33 ± 0.01	1109 ± 126		
−400	0.18 ± 0.00	3166 ± 161		

E/mV	R_{ct}/Ω g	C_{dl}/μF g^{-1}	R_{p}/Ω g	C_{p}/μF g^{-1}
Pd-modified Ni foam				
−50	0.83 ± 0.01	183,662 ± 1800	0.03 ± 0.00	217,311 ± 62,433
−100	0.67 ± 0.00	177,414 ± 1313	0.03 ± 0.00	276,556 ± 62,500
−150	0.48 ± 0.01	166,930 ± 4006	0.04 ± 0.01	620,165 ± 185,429
−200	0.42 ± 0.01	115,049 ± 4646	0.03 ± 0.01	242,973 ± 61,397
−300	0.16 ± 0.02	146,460 ± 13,357	0.04 ± 0.01	297,566 ± 87,038
−400	0.09 ± 0.01	135,222 ± 10,277	0.03 ± 0.01	267,016 ± 78,102
Ru-modified Ni foam				
−50	0.36 ± 0.01	95,558 ± 784	0.13 ± 0.01	1,504,318 ± 191,048
−100	0.25 ± 0.01	83,042 ± 1909	0.10 ± 0.01	908,603 ± 212,613
−150	0.17 ± 0.02	86,539 ± 6836	0.10 ± 0.02	348,149 ± 121,852
−200	0.19 ± 0.01	75,185 ± 1451	0.03 ± 0.01	367,532 ± 133,230
−300	0.13 ± 0.01	69,548 ± 2156	0.03 ± 0.01	184,191 ± 44,758
−400	0.09 ± 0.01	68,659 ± 3089	0.03 ± 0.01	217,240 ± 80,139

j_0 (Ni foam) = 1.4×10^{-6} A cm^{-2}.
j_0 (Ni foam/Pd) = 2.2×10^{-5} A cm^{-2}.
j_0 (Ni foam/Ru) = 8.2×10^{-5} A cm^{-2}.

Fig. 4. a) Equivalent circuit model used for fitting the impedance data for pure Ni foam electrodes, obtained in 0.1 M NaOH. The circuit includes a constant phase element (CPE) for distributed capacitance; R_{ct} and C_{dl} (as CPE$_{dl}$) elements correspond to the HER charge-transfer resistance and double-layer capacitance components, and R_{sol} is solution resistance; b) two CPE-R element equivalent circuit model used for fitting the impedance data for Pd and Ru-modified Ni foam electrodes, obtained in 0.1 M NaOH. The circuit includes two constant phase elements (CPEs) to account for distributed capacitance; R_{p} and C_{p} (as CPE$_{p}$) elements correspond to the resistance and capacitance components of an electrode porosity response; c) equivalent circuit for H UPD adsorption process (2 × CPE-modified), exhibiting Faradaic pseudocapacitance, C_{pH} (as CPE$_{pH}$) charged via a Faradaic resistance, R_{H} in a parallel combination with the double-layer capacitance, C_{dl} (as CPE$_{dl}$).

"depressed" semicircle observable throughout the high and intermediate frequency regions in the Nyquist plot together with a capacitive line, but at an inclination to the Z' axis different from 90° at sufficiently low frequencies (see Figs. 4c and 6, and Table 2 for details).

The recorded Faradaic charge-transfer resistance, R_{H} (parameter that is proportional to the inverse of the exchange rate for the process of UPD of H) significantly increased from 1.02 to 13.42 Ω g (ca. 424 to 5582 Ω cm^2, assuming the C_{dl}-approximated active surface area of the Ni foam electrode) for the studied potential range: 50–150 mV RHE. A dramatic increase of the R_{H} parameter (most likely due to enhanced interaction of surface co-adsorbed species, e.g. alkaline electrolyte impurities or oxygen containing species) follows simultaneous reduction of H adsorption pseudocapacitance, C_{pH} parameter from 789 mF g^{-1} at 50 mV to reach 710 mF g^{-1} at 150 mV. On the other hand, the recorded double-layer capacitance, C_{dl} parameter ranged from 98,006 to 234,961 μF g^{-1} for the same potential span. Rapidly increased values of the C_{dl} parameter (beyond these recorded on this electrode for the HER in Table 1) implied considerable inclusion of the hydrogen adsorption component. Also, dimensionless φ_4 and φ_5 parameters of the CPE circuit (see Fig. 4c) varied between: 0.80–0.92 and 0.76–0.94, respectively.

However, it should be noted that the presented here kinetic data for the process of UPD of H on the Ru-modified Ni foam material should by no means be compared to any existing record, produced with perfectly flat and homogeneous surfaces, for example on single-crystal electrodes (see e.g. Refs. [44,45,47,48]). However, the recorded and discussed here qualitative results gave significant evidence for the presence of Ru and Pd (results not shown for the reason stated abov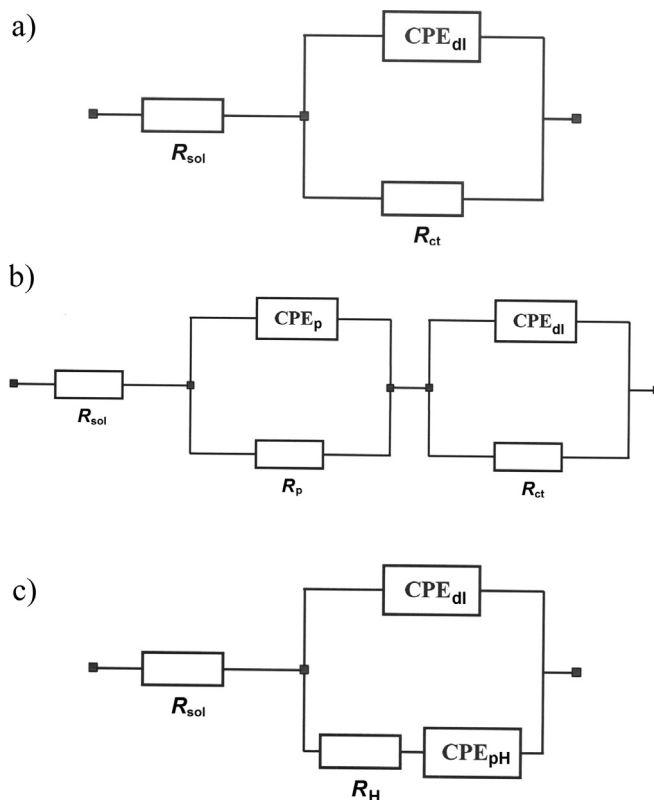e) elements on the surface of nickel foam substrate, where operational range of electrode potential was sufficiently narrow to prevent anodic dissolution of these catalytic additives.
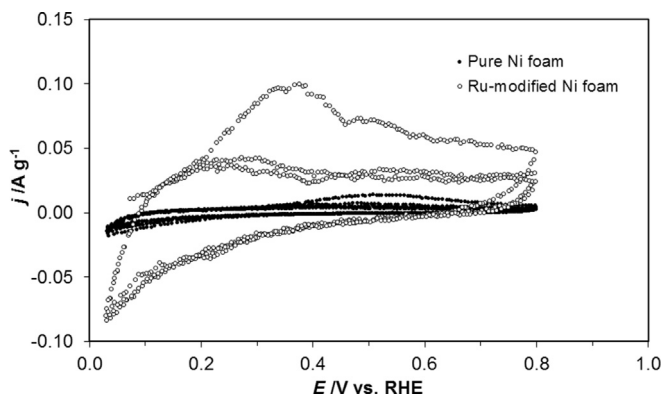

Fig. 5. Cyclic voltammograms recorded for pure Ni foam and Ru-modified Ni foam electrodes in 0.1 M NaOH, carried-out at a sweep rate of 50 mV s^{-1} for potentials positive to the HER range (small, but clearly discernible H$_2$ evolution tails along with H oxidation regions could be identified).
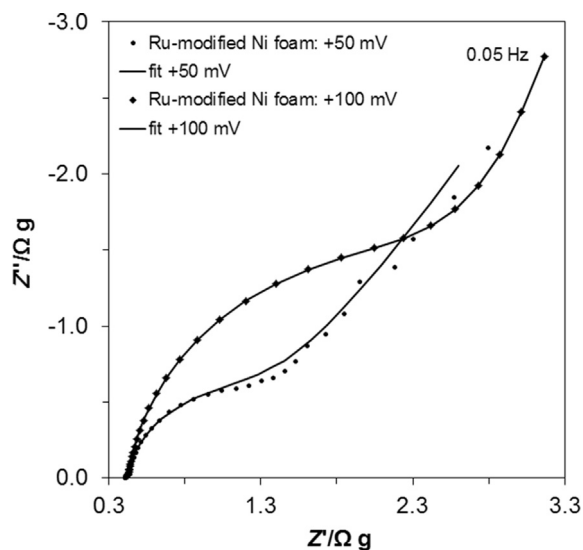
Fig. 6. Complex-plane impedance plots for the process of UPD of H on Ru-modified Ni foam electrode surface in contact with 0.1 M NaOH, recorded at room temperature for the stated potential values (vs. RHE). The solid lines correspond to representation of the data according to the equivalent circuit shown in Fig. 4c.

3.4. HER characterization by steady-state Tafel polarization curves

The kinetic results discussed above are in good agreement with these of the potentiostatic Tafel polarizations, presented in Fig. 7. In fact, radical enhancement of the HER behaviour upon introduction of catalytic amounts of Pd and Ru elements into Ni foam structure could clearly be observed over the kinetically-controlled, low overpotential region in Fig. 7. The recorded cathodic slopes (parameter b_c, see caption to Fig. 7) approached 138, 65 and 84 mV dec^{-1} for the baseline Ni foam, the Pd and the Ru-modified Ni foam catalyst materials, respectively. Significant change of the cathodic Tafel slope came in-line with facilitation of the exchange current-density parameter. Hence, the Tafel-based values of the j_0 parameter for the HER amounted to 1.3×10^{-6}, 1.1×10^{-5} and 1.4×10^{-5} A cm^{-2} for the unmodified Ni foam, the Pd and the Ru-activated nickel foam electrodes, correspondingly. It should be stressed however that significant difference between the Tafel-calculated and the impedance-derived values of the j_0 parameter for the ruthenium-modified Ni foam electrode (see Table 1 again) most likely results from inferior quality of the Tafel fit. As, a linear Tafel region for the Ru-modified Ni foam electrode was not very well pronounced in this plot (compare all three Tafel curves in Fig. 7), one should refer to the impedance-derived j_0 as much more reliable value of the exchange current-density parameter for this catalyst material. Simultaneously, for a fixed overpotential value of -100 mV, the recorded current-densities came to 7.8×10^{-6}, 7.9×10^{-5} and 1.4×10^{-4} A cm^{-2} for the unmodified, the Pd-modified and the Ru-activated Ni foam catalysts, respectively. Correspondingly, at the overpotential of -300 mV the resultant
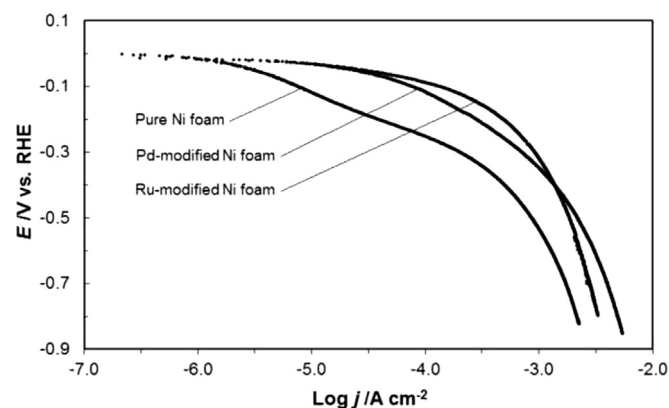
Table 2
Resistance and capacitance parameters for the process of UPD of H on Ru-modified Ni foam electrode surface in contact with 0.1 M NaOH, obtained by fitting the equivalent circuit shown in Fig. 4c to the impedance data (reproducibility below 5%, $\chi^2 = 3 \times 10^{-4}$ to 2×10^{-3}).

E/mV	R_H/Ω g	C_{dl}/μF g^{-1}	C_{pH}/mF g^{-1}
50	1.02 ± 0.07	$98,006 \pm 6664$	789 ± 21
100	2.97 ± 0.07	$159,591 \pm 2553$	909 ± 23
150	13.42 ± 0.18	$234,961 \pm 1833$	710 ± 128

Fig. 7. Quasi-potentiostatic cathodic polarization curves (recorded at a rate of 0.5 mV s^{-1}) for the HER on pure Ni foam, Pd and Ru-modified Ni foam electrode surfaces, carried-out in 0.1 M NaOH solution (appropriate iR correction was made based on the solution resistance derived from the impedance measurements); calculated Tafel slopes, $b_c = 138$, 65 and 84 mV dec^{-1} for baseline Ni foam, Pd-based and Ru-modified Ni foam cathodes.

current-densities reached: 2.1×10^{-4}, 7.1×10^{-4} and 9.2×10^{-4} A cm^{-2}.

With respect to the derived exchange current-densities, Tafel slopes and the recorded Tafel plots, the results presented in this paper compare quite well with those of other HER works (see Refs. [6,8,17,18,29,49–51]), performed on analogous catalyst materials, including highly-porous Ni-based electrodes. However, as some of these works [18,29,50,51] clearly reported their electrochemical results with respect to the base (unmodified) geometric surface area, the observed there HER activities were apparently radically enhanced (several orders in magnitude). On the contrary, the results presented in this work were "normalized" based on the surface area estimates given through interfacial capacitance measurements (see paragraph 3.2. above for details). In fact, for a spongy-type entity such as Ni foam electrode, electrochemical results might also be conveniently presented as per electrode mass instead of its surface area, which is very difficult to be properly estimated.

4. Conclusions

Palladium and ruthenium nano deposits (at *ca.* 0.1 wt.%) on the surface of cathodically activated pure Ni foam material radically enhanced catalytic activity of baseline material towards cathodic evolution of hydrogen in alkaline solution (especially observed over kinetically-controlled overpotential range). The above is primarily related to superior HER activity of catalytic additives (Pd and especially Ru), in addition to the resultant, substantial modification of electrochemically active surface for these catalyst materials. In addition, both Pd and Ru-modified nickel foam electrodes exhibited electrochemical impedance behaviour characteristic of a porous electrode structure (contrast to the behaviour observed on pure nickel foam electrode) with two partial semicircles present in the Nyquist impedance spectra.

Finally, the results obtained in this work clearly indicated substantial opportunities for Ni foam-modified cathode materials in commercial alkaline water electrolysers.

References

[1] B.E. Conway, B.V. Tilak, Adv. Catal. 38 (1992) 1.
[2] J.Y. Huot, L. Brossard, Int. J. Hydrogen Energy 12 (12) (1987) 821.
[3] H.E.G. Rommal, P.J. Morgan, J. Electrochem. Soc. 135 (2) (1988) 343.
[4] D.M. Soares, O. Teschke, I. Torriani, J. Electrochem. Soc. 139 (1) (1992) 98.

[5] N. Krstajic, M. Popovic, B. Grgur, M. Vojnovic, D. Sepa, J. Electroanal. Chem. 512 (2001) 16.
[6] M.A. Dominguez-Crespo, E. Ramirez-Meneses, A.M. Torres-Huerta, V. Garibay-Febles, K. Philippot, Int. J. Hydrogen Energy 37 (2012) 4798.
[7] M. Mitov, E. Chorbadzhiyska, R. Rashkov, Y. Hubenova, Int. J. Hydrogen Energy 37 (2012) 16522.
[8] M.A. Dominguez-Crespo, A.M. Torres-Huerta, B. Brachetti-Sibaja, A. Flores-Vela, Int. J. Hydrogen Energy 36 (2011) 135.
[9] B. Pierozynski, L. Smoczynski, J. Electrochem. Soc. 156 (9) (2009) B1045.
[10] B. Pierozynski, Int. J. Electrochem. Sci. 6 (2011) 63.
[11] B. Pierozynski, Int. J. Hydrogen Energy 38 (2013) 7733.
[12] R. Solmaz, A. Gundogdu, A. Doner, G. Kardas, Int. J. Hydrogen Energy 37 (2012) 8917.
[13] H. He, H. Liu, F. Liu, K. Zhou, Surf. Coat. Technol. 201 (2006) 958.
[14] E. Verlato, S. Cattarin, N. Comisso, A. Gambirasi, M. Musiani, L. Vazquez-Gomez, Electrocatal. 3 (2012) 48.
[15] V. Paserin, S. Marcuson, J. Shu, D.S. Wilkinson, Adv. Eng. Mater. 6 (2004) 454.
[16] S. Inazawa, A. Hosoe, M. Majima, K. Nitta, Sci. Tech. Rev. 71 (2010) 23.
[17] I. Bianchi, E. Guerrini, S. Trasatti, Chem. Phys. 319 (2005) 192.
[18] L. Vazquez-Gomez, S. Cattarin, P. Guerriero, M. Musiani, Electrochim. Acta 53 (2008) 8310.
[19] P. Kim, J.B. Joo, W. Kim, J. Kim, I.K. Song, J. Yi, J. Power Sources 160 (2006) 987.
[20] Y. Suo, I.M. Hsing, J. Power Sources 196 (2011) 7945.
[21] A. Dutta, S.S. Mahapatra, J. Datta, Int. J. Hydrogen Energy 36 (2011) 14898.
[22] R.M. Modibedi, T. Masombuka, M.K. Mathe, Int. J. Hydrogen Energy 36 (2011) 4664.
[23] B. Beyribey, B. Corbacioglu, Z. Altin, G. U. J. Sci. 22 (4) (2009) 351.
[24] J.R. Macdonald, Impedance Spectroscopy, Emphasizing Solid Materials and Systems, John Wiley & Sons, New York, 1987.
[25] T. Pajkossy, J. Electroanal. Chem. 364 (1994) 111.
[26] B.E. Conway, B. Pierozynski, J. Electroanal. Chem. 622 (2008) 10.
[27] A. Lasia, A. Rami, J. Appl. Electrochem 22 (1992) 376.
[28] L. Chen, A. Lasia, J. Electrochem. Soc. 138 (1991) 3321.
[29] C. Hitz, A. Lasia, J. Electroanal. Chem. 500 (2001) 213.
[30] C. Gabrielli, F. Huet, R.P. Nogueira, Electrochim. Acta 50 (2005) 3726.
[31] J.A. Harrison, Surf. Technol. 19 (3) (1983) 249.
[32] P. Paunovic, O. Popovski, S.H. Jordanov, A. Dimitrov, D. Slavkov, J. Serb. Chem. Soc. 71 (2) (2006) 149.
[33] S. Rausch, H. Wendt, J. Electrochem. Soc. 143 (9) (1996) 2852.
[34] T. Borucinski, S. Rausch, H. Wendt, J. Appl. Electrochem. 22 (1992) 1031.
[35] J.G. Highfield, E. Claude, K. Oguro, Electrochim. Acta 44 (1999) 2805.
[36] R.K. Shervedani, A.R. Madram, Electrochim. Acta 53 (2007) 426.
[37] S. Martinez, M. Metikos-Hukovic, L. Valek, J. Mol. Catal. A: Chem. 245 (2006) 114.
[38] A. Bewick, J.W. Russell, J. Electroanal. Chem. 142 (1982) 337.
[39] M. Elam, B.E. Conway, J. Electrochem. Soc. 135 (1988) 1678.
[40] J. Clavilier, K. El Achi, M. Petit, A. Rodes, M.A. Zamakhchari, J. Electroanal. Chem. 295 (1990) 333.
[41] J. Clavilier, A. Rodes, K. El Achi, M.A. Zamakhchari, J. Chim. Phys. 88 (1991) 1291.
[42] N. Furuya, S. Motoo, J. Electroanal. Chem. 98 (1979) 189.
[43] M.H. Martin, A. Lasia, Electrochim. Acta 53 (2008) 6317.
[44] H. Duncan, A. Lasia, Electrochim. Acta 52 (2007) 6195.
[45] B. Łosiewicz, M. Martin, C. Lebouin, A. Lasia, J. Electroanal. Chem. 649 (2010) 198.
[46] J. Prakash, H. Joachin, Electrochim. Acta 45 (2000) 2289.
[47] S. Morin, H. Dumont, B.E. Conway, J. Electroanal. Chem. 412 (1996) 39.
[48] S.Y. Qian, B.E. Conway, G. Jerkiewicz, Int. J. Hydrogen Energy 25 (2000) 539.
[49] I. Herraiz-Cardona, E. Ortega, L. Vazquez-Gomez, V. Perez-Herranz, Int. J. Hydrogen Energy 37 (2012) 2147.
[50] L. Vazquez-Gomez, S. Cattarin, P. Guerriero, M. Musiani, Electrochim. Acta 52 (2007) 8055.
[51] A.L. Antozzi, C. Bargioni, L. Iacopetti, M. Musiani, L. Vazquez-Gomez, Electrochim. Acta 53 (2008) 7410.